A Novel Approach to Well-Aligned TiO_2 Nanotube Arrays and Their Enhanced Photocatalytic Performances

Weixin Zhang, Gongde Chen, Zeheng Yang, and Chunyan Zeng
School of Chemical Engineering, Hefei University of Technology, Hefei, Anhui 230009, P.R. China

Anhui Key Laboratory of Controllable Chemical Reaction and Material Chemical Engineering, Hefei, Anhui 230009, P.R. China

DOI 10.1002/aic.13985
Published online January 8, 2013 in Wiley Online Library (wileyonlinelibrary.com)

A simple route has been developed to prepare well-aligned TiO_2 nanotube arrays, which is based on outward coating of TiO_2 and inward etching of $Cu(OH)_2$ nanorod templates. Effects of annealing temperature and time on the crystal size and crystallinity of TiO_2 nanotube arrays and photocatalytic activities of TiO_2 nanotube arrays for degradation of Rhodamine B in aqueous solution have been investigated. The results indicate that the TiO_2 nanotube arrays annealed at 500°C for 2 h possessed an enhanced photocatalytic activity in comparison with the TiO_2 nanotube arrays without post heating and commercial anatase TiO_2 nanoparticle film and presented a good life cycle performance. Scale-up of the process has also been demonstrated. Our work opens a new avenue to fabricate free-standing TiO_2 nanotube arrays and demonstrates an excellent photocatalytic performance of the anatase TiO_2 nanotube arrays for wastewater treatment. © 2013 American Institute of Chemical Engineers *AIChE J*, 59: 2134–2144, 2013
Keywords: TiO_2, nanotube arrays, Rhodamine B, photocatalysis, degradation

Introduction

Due to their chemical stability, nontoxicity, low cost, and some other remarkable physical and chemical properties, TiO_2 nanostructures have found wide applications in many domains including environment protection,[1–3] gas sensing, and[4,5] energy storage and conversion.[6–8] A number of synthetic strategies have been reported to fabricate TiO_2 nanosheets,[9] nanorods,[10] nanotubes,[11,12] nanospheres,[13] and so forth. Recently, many dazzling nanostructure arrays have been fabricated on some useful substrates to introduce and realize their functionalities.[14] Among them, TiO_2 nanotube arrays have attracted significant attention given their characteristics of high specific surface area, excellent charge transfer properties,[15] easy operation and recovery, and convenient recycling in practical applications. These advantages of TiO_2 nanotube arrays overcome the vital technical problems encountered by colloidal and particulate TiO_2, such as separation, particle aggregation, and the problematic use in continuous flow process.

In the past decades, a series of methods have been proposed to immobilize TiO_2 on the solid substrates to overcome the problems that powder-form TiO_2 faces with, including sol-gel dip-coating,[16] sputtering,[17] chemical vapor deposition,[18] and so forth. However, compared with the TiO_2 powder, its film usually shows a low photocatalytic efficiency because of an inevitable decrease of its active surface areas and a limited mass diffusion in solution.[16] TiO_2 nanotube arrays have well-aligned tubular structure and porous surface, which may provide a large active surface area, short diffusion path from bulk solution to active surface area, and an efficient light absorption and separation of photogenerated carriers.[19] Therefore, they can be expected to have enhanced photocatalytic activity.

In 1999, Zwilling et al.[20] first reported self-organized TiO_2 nanotube layers fabricated by electrochemical titanium anodization. Since then, this approach has mainly been used as the synthetic strategy for TiO_2 nanotube arrays. Macak et al.[19] prepared self-organized TiO_2 nanotube array layer with inner diameters of 45–100 nm by anodization of Ti foil, which was post heated at 450°C over 3 h to obtain anatase phase. They found that anatase TiO_2 nanotube layers exhibited a better photocatalytic activity for the decomposition of organic azo dyes in comparison with a compacted TiO_2 nanopowder layer. Wang et al.[21] synthesized highly aligned TiO_2 nanotube arrays by a liquid-phase deposition method. Anodic aluminum oxide template was immersed in $(NH_4)_2TiF_6$ aqueous solution of 0.5 mol/L at 60°C for 10 min. TiO_2 nanotube arrays with an outer diameter of 200 nm and an inner diameter of 100 nm formed *in situ* in the inner side of the templates. Post heat treatment at 400°C for 4 h was employed to produce anatase-type TiO_2, which was used as a photocatalyst to degrade methylene blue.

We have reported an inward chemical lithography route to prepare Cu_7S_4 nanotube arrays[22] and double-walled Cu_7S_4 and $Cu_{2-x}Se$ nanotube arrays[23] based on $Cu(OH)_2$ nanorod arrays grown on copper foil. Herein, we demonstrate an

Additional Supporting Information may be found in the online version of this article.

Correspondence concerning this article should be addressed to W. Zhang at wxzhang@hfut.edu.cn.

alternative chemical way to synthesize TiO_2 nanotube arrays at room-temperature using $Cu(OH)_2$ nanorod arrays as the templates. The influence of annealing temperature and time on the crystallite size and crystallinity of the TiO_2 nanotube arrays has also been investigated. Moreover, we have examined the photocatalytic activities of the obtained anatase TiO_2 nanotube arrays in the degradation of RhB dye in aqueous solution, and compared it with that of TiO_2 nanotube arrays obtained without post heating and TiO_2 film made from commercial anatase TiO_2 powder. The kinetic modeling for the degradation of RhB has been developed. To explore the potential application in wastewater treatment, the life cycle and scale-up performance of the anatase TiO_2 nanotube arrays have been investigated.

Experimental Section

Materials

All chemicals were purchased from Sinopharm Chemical Reagent Co., Ltd, China and used as-received without any further purification. Stock solutions of sodium hydroxide (10 mol/L) and ammonia persulfate (1 mol/L) were prepared by dissolving NaOH and $(NH_4)_2S_2O_8$ in distilled water, respectively. Tetra-n-butyl titanate ($Ti(OC_4H_9)_4$) was dissolved in ethanol as titanium source. Ammonia solution (25 wt %) and Copper foil in high-purity (99.99%) were also used. Commercial TiO_2 powder was used for a comparison experiment.

Synthesis of $Cu(OH)_2$ nanorod array templates

The details to synthesize $Cu(OH)_2$ nanorod arrays grown on copper foil were described in our previous papers.[22,23] Typically, an aqueous solution was prepared in a 60-mL bottle by mixing 10 mL of distilled water, 2 mL of NaOH solution (10 mol/L), 1 mL of $(NH_4)_2S_2O_8$ solution (1 mol/L), and 1.0 mL of ammonia solution (25 wt %). A piece of copper foil ($10 \times 10 \times 0.25$ mm^3) which had been ultrasonically cleaned in acetone, absolute ethanol, and distilled water in turn was immersed in as-prepared solution at room-temperature. After 50 min, the copper foil covered with a blue film was taken out, rinsed with distilled water and absolute ethanol, and dried in air.

Synthesis of $Cu(OH)_2/TiO_2$ core/sheath nanorod arrays

$Ti(OC_4H_9)_4$ (1 mL) was dissolved in 5 mL of ethanol to make a solution. $Cu(OH)_2$ nanorod arrays grown on copper foil were then immersed in the solution. After 10 min, the sample was taken out of the solution and placed in air.

Synthesis of TiO_2 nanotube arrays

The sample of $Cu(OH)_2/TiO_2$ core/sheath nanorod arrays was immersed in a 10 mL of ammonia aqueous solution (12.5 wt %) for 16 h to dissolve the inner $Cu(OH)_2$ cores. Then, the sample was taken out, rinsed with distilled water and ethanol, and dried in air. The obtained sample was annealed in a nitrogen atmosphere.

Fabrication of commercial TiO_2 powder film

Commercial TiO_2 powder and polyvinylidene fluoride as a binder in the weight ratio of 20:1 were mixed in a solvent of *N*-methyl pyrrolidinone. The obtained homogenous slurry was cast onto copper foil to form a film by a doctor blade method, followed by evaporation of the solvent in a mild heating condition. Then, the film was cut into square pieces with the same film area (10×10 mm^2) as that of the TiO_2 nanotube arrays.

Characterization of the samples

The samples were characterized by X-ray powder diffraction (XRD) in a Rigaku D/max-γB X-ray diffractometer with a Cu kα radiation source ($\lambda = 0.154178$ nm) operated at 40 kV and 80 mA. The scanning time of XRD measurement for every sample was 15 min. The step width was 0.02 degree. The morphologies and structures of the samples were characterized using field-emission scanning electron microscope (FESEM; FEI Sirion-200), scanning electron microscope (SEM; JSM-6490), transmission electron microscope (TEM; Hitachi H-800), and high-resolution TEM (HRTEM; JEM-2100F), respectively. The TEM and HRTEM measurements were both performed at an accelerating voltage of 200 kV. Photoluminescence (PL) spectra were recorded at room-temperature on a fluorescence spectrophotometer (Hitachi F-4500) with a Xenon lamp (150 W) as the excitation source. Both entrance and exit slits were 5.0 nm. The scanning speed was 1200 nm/min, and the scanning range was from 375 to 750 nm.

Adsorption-desorption isotherms of N_2 were obtained on a Quantachrome NOVA 2200e surface area and pore-size analyzer at liquid nitrogen temperature. The specific surface area of the samples was calculated by following the multipoint Brunauer–Emmett–Teller (BET) procedure, and average pore diameters were determined by the Barrett–Joyner–Halenda method. Before the measurement, each sample was degassed at 120°C for over 4 h.

Photocatalytic activity measurement

The photocatalytic activities of the samples were evaluated by the degradation of RhB in aqueous solution under a UV light irradiation at a distance of 10 cm. A high-pressure Hg lamp (predominant wavelength $\lambda = 365$ nm, 300 W) served as the UV light source. The photocatalytic reactions were carried out in a quartz cuvette. TiO_2 nanotube arrays or a commercial TiO_2 powder film were vertically immersed in 1 mL of RhB aqueous solution with an initial concentration of 4 mg/L and faced to the light source. Before irradiation, the system was placed in the dark for 30 min to achieve adsorption equilibrium. Every other 30 min, the photocatalyst was removed from the cuvette. After a couple of shakes, the cuvette was placed in the fluorescence spectrophotometer, and residual RhB concentration was determined by detecting its characteristic emission wavelength at 586 nm. The excitation wavelength was 350 nm. Shortly after that, the photocatalyst was immersed in the solution again for further photocatalytic reaction. Every measuring process took less than 1 min.

Results and Discussion

Composition, morphology, and structure of the TiO_2 nanotube arrays

Figure 1 shows the XRD patterns of the products prepared in the evolution process. In Figure 1a, a series of diffraction peaks marked with ▲ can be indexed to the orthorhombic $Cu(OH)_2$ (JCPDS 13-0420), except those with *, which come from the copper substrate. The XRD pattern of $Cu(OH)_2/TiO_2$ core/sheath sample presented in Figure 1b is similar to that in Figure 1a, and no obvious characteristic

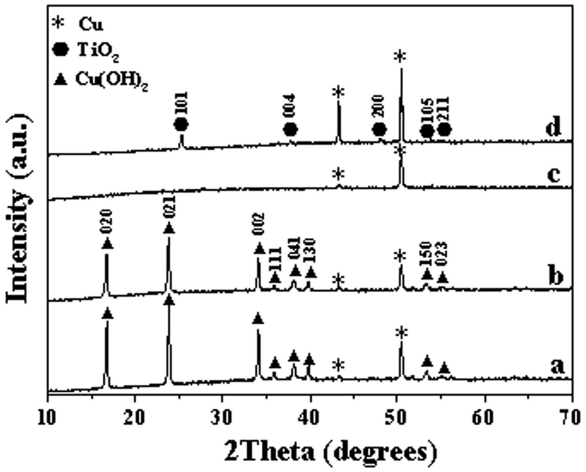

Figure 1. XRD patterns of the samples on a copper substrate.

(a) $Cu(OH)_2$ nanorod arrays, (b) $Cu(OH)_2/TiO_2$ core/sheath nanorod arrays, (c) TiO_2 nanotube arrays without post heating, and (d) TiO_2 nanotube arrays annealed at 500°C for 4 h.

peak can be observed for TiO_2, indicating a low crystallinity of the TiO_2 layer obtained from the hydrolysis of $Ti(OC_4H_9)_4$.[24,25] After dissolution of the $Cu(OH)_2$ cores, only reflections assigned to Cu are presented in Figure 1c, further confirming that the TiO_2 nanotubes without post heating were poorly crystallized. Through post heat treatment operated in a nitrogen atmosphere at 500°C for 4 h, the characteristic planes of anatase TiO_2 phase appear in Figure 1d. All the peaks marked with • can be indexed to anatase-type TiO_2 (JCPDS 21-1272). Commercial TiO_2 powder used in this work for a comparison of photocatalytic activity was also characterized, and found to be pure anatase phase. Its XRD pattern is presented in Figure S1 (see Supporting Information).

The SEM images of $Cu(OH)_2$ nanorod arrays, and $Cu(OH)_2/TiO_2$ core/sheath nanorod arrays are presented in Figure 2. As observed in Figure 2a, the $Cu(OH)_2$ nanorods had diameters of 200–500 nm and lengths up to 10–15 μm. Clearly, the templates of $Cu(OH)_2$ nanorod arrays were well-aligned. Figure 2b shows the top view of $Cu(OH)_2/TiO_2$ core/sheath nanorod arrays, which presents a similar morphology to the array of $Cu(OH)_2$ nanorod templates.

After the dissolution of $Cu(OH)_2$ core, TiO_2 nanotube arrays were obtained. Figure 3 shows the FESEM and the corresponding TEM images of the samples. The top view FESEM image of the TiO_2 nanotube arrays without post heating is displayed in Figure 3a. As clearly shown, large scale of TiO_2 nanotube arrays with similar morphology to the $Cu(OH)_2$ templates were prepared on copper substrate (also shown in Supporting Information, Figure S2a). The TiO_2 nanotubes were well-aligned and had close tips, which can also be observed in Supporting Information, Figures S2b, c. To examine the hollow interiors of these nanostructures, the sample was scraped slightly and some of the close tips were cut off. One magnified TiO_2 nanotube with a broken tip can be clearly seen in the inset of Figure 3a and in Supporting Information, Figure S2d, indicating that the as-prepared TiO_2 nanotube arrays possessed a sheath-like nanostructure. Figure 3b presents the light and dark contrast in the TEM image of the TiO_2 nanotubes without post heating, which further confirms the sheath-like structure of the nanotubes. From the FESEM and TEM results, it can be observed that the TiO_2 nanotubes ranged from 200 to 500 nm in diameter. The film thickness of the TiO_2 nanotube arrays was about 15 μm, which can be obtained from the cross-sectional SEM image in Supporting Information, Figure S3a.

Figure 3c manifests the TiO_2 nanotube arrays on copper foil after heat treatment. It is clear to see that array of the TiO_2 nanotubes after post heating was nearly vertically aligned on the copper substrate. TiO_2 nanotubes were intact without any sign of breakage. The corresponding TEM image in Figure 3d exhibits the tubular structure of TiO_2, which is in good agreement with Figure 3b.

The FESEM image of the commercial TiO_2 powder is displayed in Figure 3e. As observed, the film was composed of agglomerated nanoparticles with a size of about 100 nm, which is consistent with the TEM result presented in Figure 3f. The film thickness of the commercial TiO_2 nanoparticles was about 10 μm, which can be obtained from the sectional SEM image of the commercial TiO_2 powder film presented in Supporting Information, Figure S3b.

Formation process of the anatase TiO_2 nanotube arrays

To investigate the formation process of the anatase TiO_2 nanotube arrays, temporal evolution has been tracked by TEM observation. Figure 4a shows the TEM image of the original $Cu(OH)_2$ nanorod, with a diameter of about 500 nm.

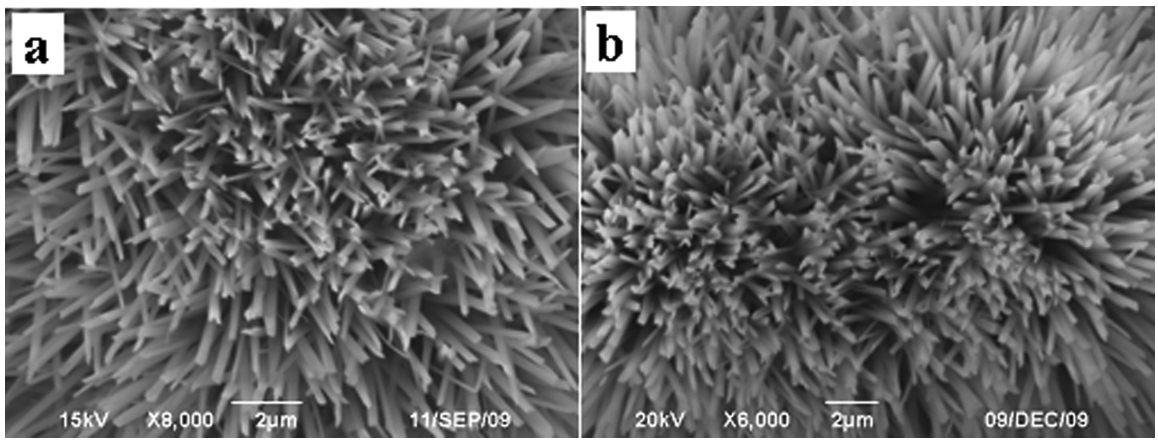

Figure 2. SEM images of (a) $Cu(OH)_2$ nanorod arrays and (b) $Cu(OH)_2/TiO_2$ core/sheath nanorod arrays.

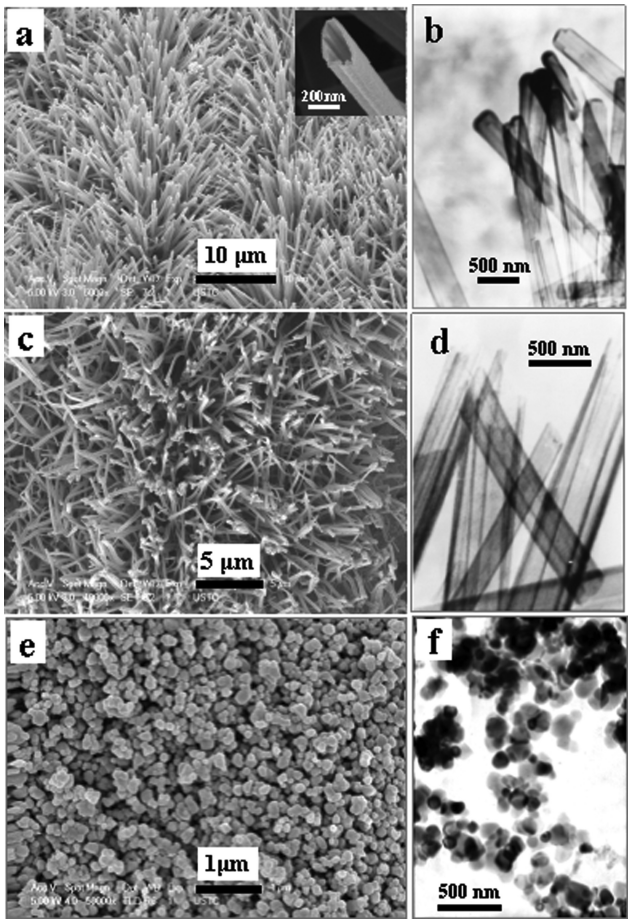

Figure 3. FESEM and TEM images of the samples.

(a, b) TiO_2 nanotube arrays without post heating, (c, d) TiO_2 nanotube arrays annealed at 500°C for 4 h, and (e, f) commercial anatase TiO_2 powder film.

After the process of adsorption and hydrolysis of $Ti(OC_4H_9)_4$, a uniform TiO_2 layer was formed on the surface of the $Cu(OH)_2$ nanorod. The edge contrast can be seen in Figure 4b, which reveals the formation of $Cu(OH)_2/TiO_2$ core/sheath structure. The thickness of as-formed TiO_2 sheath is estimated to be about 30 nm. When the $Cu(OH)_2/TiO_2$ core/sheath nanorod was immersed in a 10 mL of ammonia aqueous solution (12.5 wt %) for about 16 h, the $Cu(OH)_2$ core was dissolved and TiO_2 nanotube was obtained. As shown in Figure 4c, the sharp contrast between the wall (dark) and the interior (pale) indicates a hollow structure. It is evident that the tip of the nanotube was closed. The rings presented in the selected area electron diffraction (SAED) pattern of the TiO_2 nanotube without post heating are not clear except the (101) plane, revealing its low crystallinity. Figure 4d presents the TEM image of one TiO_2 nanotube after post heat treatment, which shows a well-retained tubular structure. Diffraction rings corresponding to (101), (004), and (211) planes of anatase TiO_2 are observed in the SAED, indicating polycrystalline structure of the anatase TiO_2 nanotube.

Effect of annealing temperature on the TiO_2 nanotube arrays

Figure 5a shows the XRD patterns of the TiO_2 nanotubes annealed at temperatures ranging from 300 to 600°C for 4 h. For comparison, the XRD pattern of the sample without post heating is also presented, and there is no observable peak. For the sample annealed at 300°C, its XRD pattern is similar to that without post heating, which implies that TiO_2 was not crystallized yet at this temperature. When the temperature increased to 400°C, a tiny diffraction peak (framed by dash lines) emerged at 25.3°, which can be assigned to the (101) plane of anatase TiO_2 (JCPDS 21-1272). This evidence indicates that anatase phase began to form at around 400°C. When the annealing temperature went up to 500°C, all the peaks marked with A can be indexed to anatase phase TiO_2. Additionally, the relative intensity of the diffraction peaks became stronger, indicating the increase of crystallinity. Further increasing the annealing temperature to 600°C led to appearance of rutile TiO_2 (JCPDS 21-1276). The sample obtained at this temperature contained a mixing phase, but the predominant phase was still anatase.

The results presented in Figure 5b give clear evidence that the annealing temperature affected the photocatalytic performance of the TiO_2 nanotube arrays. After 180 min of irradiation, 74.1% of RhB was degraded by the TiO_2 nanotube arrays annealed at 300°C for 4 h. The degradation ratio increased to 83.2, 87.9, and 87.3% for the samples annealed at 400, 500, and 600°C for 4 h, respectively. It can be seen that the photocatalytic activities of the TiO_2 nanotube arrays were improved with the increase of annealing temperature from 300 to 500°C, exhibiting a similar trend to the previous report,[26] which investigated a photoelectrocatalytic activity of the TiO_2 nanotube arrays electrode annealed at various temperatures for azo dye degradation. However, there was

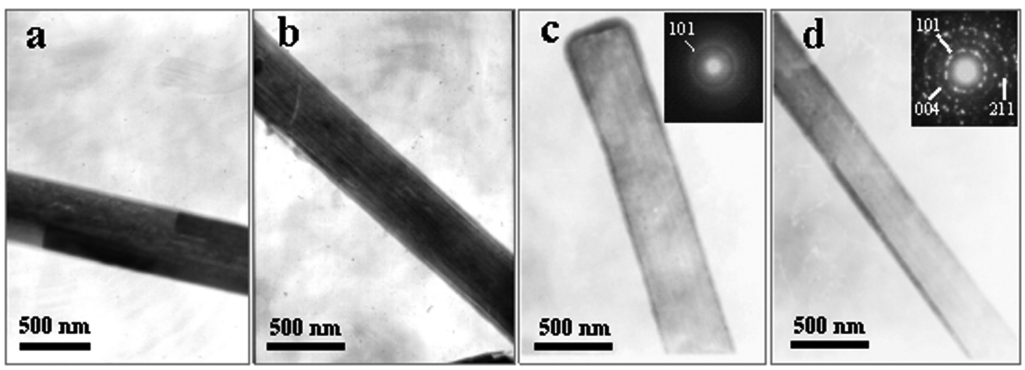

Figure 4. TEM images for the evolution process of the anatase TiO_2 nanotube.

(a) $Cu(OH)_2$ nanorod, (b) $Cu(OH)_2/TiO_2$ core/sheath nanorod, (c) TiO_2 nanotube without post heating (inset: the corresponding ED pattern), and (d) TiO_2 nanotube annealed at 500°C for 4 h (inset: the corresponding ED pattern).

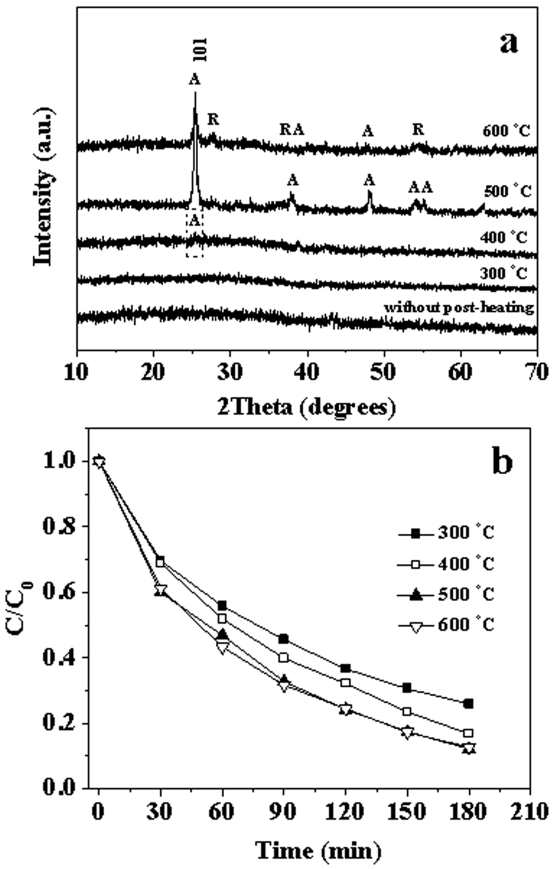

Figure 5. (a) XRD patterns of the TiO_2 nanotubes without post heating and annealed at varying temperatures for 4 h; (b) the variation of the relative concentration of RhB as a function of UV light irradiation time in the presence of the TiO_2 nanotube arrays as the photocatalysts which were annealed at varying temperatures for 4 h.

(All samples for XRD tests were scraped from copper substrates. The photocatalytic systems were placed in the dark for 30 min beforehand.)

no further improvement in the photocatalytic activity when the annealing temperature was changed from 500 to 600°C. The two samples showed comparable photocatalytic activity with each other.

It should be pointed out that the concentration of RhB decreased before UV light irradiation because of the adsorption effect on the surface of TiO_2 nanotube arrays. Adsorption experiments in the dark showed that RhB concentration leveled off after 30 min of adsorption on the TiO_2 nanotube arrays. So, 30 min was chosen as the adsorption time for reaching the equilibrium. The values of the adsorption ratio at 30 min were 16.0, 14.5, 6.6, and 4.8%, respectively, for the TiO_2 nanotube arrays annealed at the temperature varying from 300 to 600°C for 4 h. This tendency may result from the surface area decrease of the TiO_2 nanotube arrays.

According to the XRD results in Figure 5a and the SAED patterns presented in Supporting Information, Figure S4, the crystallinity of the TiO_2 nanotube has been improved with the increase of the annealing temperature from 300 to 500°C, which may contribute to the increasingly enhanced photocatalytic activity of the TiO_2 nanotube arrays. When the annealing temperature reached up to 600°C, a small amount of rutile phase formed due to the partial transformation from anatase to rutile. However, anatase TiO_2 is commonly considered to be much more photoactive than rutile because of a superior capacity of uptaking O_2.[27] Therefore, partial phase transformation at a relatively high temperature may explain why no further improvement of the photocatalytic performance was obtained when the annealing temperature increased from 500 to 600°C.

Compared with the sample annealed at 600°C, the TiO_2 nanotube arrays annealed at 500°C had a pure anatase phase and comparable photocatalytic performance. Moreover, they showed better crystallinity and photocatalytic performance than the samples annealed at 300 and 400°C. These merits are beneficial to the subsequent screening and optimization of the annealing parameters for TiO_2 nanotube arrays. Therefore, 500°C was chosen as the annealing temperature for the following investigation.

Effect of annealing time on the TiO_2 nanotube arrays

Figure 6a shows the XRD patterns of the samples annealed at 500°C for 1–6 h. It can be seen that all indexed peaks can be assigned to anatase TiO_2 (JCPDS 21-1272). With the annealing time increasing from 1 to 4 h, the

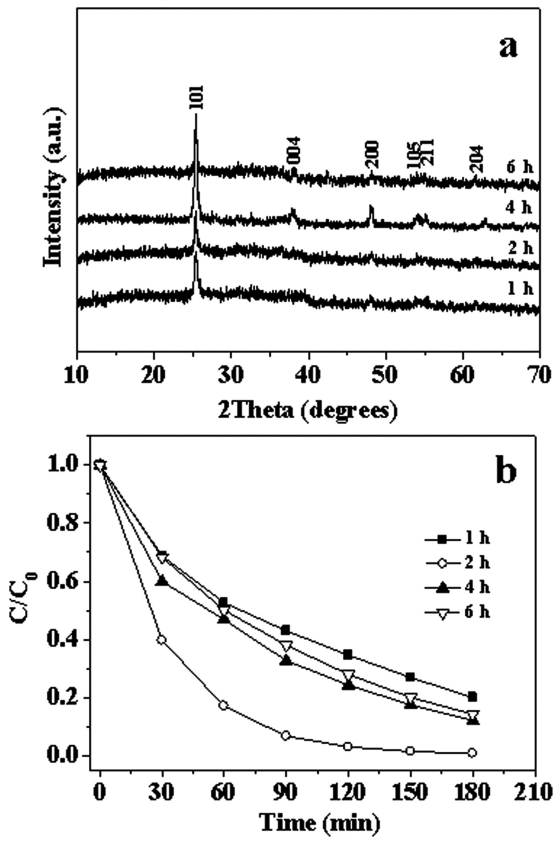

Figure 6. (a) XRD patterns of the TiO_2 nanotubes annealed at 500°C for varying time; (b) the variation of the relative concentration of RhB as a function of UV light irradiation time in the presence of the TiO_2 nanotube arrays as the photocatalysts which were annealed at 500°C for varying time.

(All samples for XRD tests were scraped from copper substrates. The photocatalytic systems were placed in the dark for 30 min beforehand).

relative intensity of the diffraction peaks increased, indicating the improvement of the samples' crystallinity. However, when the annealing time was prolonged to 6 h, the intensity of the major peaks decreased. One possible reason for this phenomenon is that an underlying tendency for phase transformation from anatase to rutile might be underway. The influence of the annealing time on average crystallite sizes can be deduced from the corresponding XRD patterns. Based on the Scherrer formula, the crystallite sizes (calculated from the peak width at half height of anatase (101) plane) of the samples annealed at 500°C for 1–6 h are 20.5, 22.9, 27.7, and 31.5 nm, respectively. It is clear that the crystallite size increased with the annealing time prolonged.

Figure 6b shows the influence of the annealing time on the photocatalytic activity of the TiO_2 nanotube arrays. The degradation ratio of the samples annealed at 500°C for 1, 2, 4, and 6 h is 80.0, 99.3, 87.9, and 85.8%, respectively. It is evident that the TiO_2 nanotube arrays annealed at 500°C for 2 h presented a superior photocatalytic performance to other samples.

Normally, extending the annealing time favors the crystallization of the TiO_2 nanotube arrays, which has been confirmed by the XRD results in Figure 6a and the SAED patterns in Supporting Information, Figure S5. The photocatalytic activity increase within the first 2 h probably resulted from the increased crystallinity. However, the crystallite size increased dramatically from 22.9 to 27.7 and 31.5 nm when the annealing time was prolonged from 2 to 4 and 6 h, which can also be observed from the high-magnification TEM images of the TiO_2 nanotube in Supporting Information, Figure S5. The increase of crystal sizes might result in the decrease of their specific surface areas, which can be reflected from the decreasing adsorption effects of the TiO_2 nanotube arrays. Adsorption tests in the dark showed that with the increase of annealing time, the equilibrium adsorption ratios for these four samples were 10.3, 7.9, 6.4, and 4.4%, respectively. As well-known, there are a lot of active reaction sites on the surface of photocatalysts. Decreasing specific surface area probably led to the decrease of the number of the active sites, whose effect might far outweigh that of the increasing crystallinity. Thus, a decreased photocatalytic activity was observed for the photocatalysts annealed at 500°C for 4 and 6 h.

Based on the results presented above, the anatase TiO_2 nanotube arrays obtained at 500°C for 2 h exhibited a satisfactory photocatalytic performance. Thus, they were selected for the further investigation.

Kinetic modeling of photocatalytic degradation

The TiO_2 nanotube arrays had a film thickness of about 15 μm (see Supporting Information, Figure S3a). It is necessary to examine the mass-transfer limitations for the photocatalytic reaction of the RhB molecules. To identify whether the reaction is kinetically controlled or predominated by mass transfer, constant stirring was introduced to reduce or even eliminate the influence of external mass transfer of RhB from bulk solution to the surface of the film. The photocatalytic degradation ratio of RhB in the presence of the anatase TiO_2 nanotube arrays all reached up to 99% or so within 180 min with or without constant stirring, which indicates that the reaction was not controlled by the external mass transfer.

It is believed that internal mass-transfer resistance depends on the nature of catalyst, film thickness, film-making technique, and preheat treatment and post heat treatment of catalyst film.[28,29] In this study, the prepared TiO_2 nanotube array film was very thin (about 15 μm) and composed of free-standing TiO_2 nanotubes. Large interspace existed among well-aligned nanotubes, which can also be reflected from the extremely low catalyst loading (only 0.14 mg/cm^2) for the TiO_2 nanotube array film. According to Zhou et al.,[28] the internal mass-transfer resistance could be neglected for a low catalyst loading of 0.52 mg/cm^2. Furthermore, the interconnected top-to-bottom space among nanotubes and the nanotubular geometry of the photocatalyst can provide a shorter and easier diffusion path for RhB within the nanotube array film, compared with the convoluted porous nanoparticle film. Thus, the internal mass-transfer resistance arising from the diffusion through the TiO_2 nanotube array layer can be considered to be negligible. Because TiO_2 nanotubes had porous walls with a thickness of only 30 nm or so, the internal mass-transfer resistance from the wall diffusion is also assumed to be negligible.

Based on what has been discussed above, it can be concluded that the external and internal mass-transfer resistance are not the predominant limitation for the photocatalytic reaction. Kinetics should be the main restrictive factor for the reaction. The kinetics of heterogeneous catalysis of a liquid-solid system has frequently been described using Langmuir–Hinshelwood (L-H) model,[30,31] which can be expressed by Eq. 1

$$r = -\frac{dC}{dt} = \frac{k_r KC}{1+KC+K_s C_s} \tag{1}$$

Here, C is the concentration of the reactant, t is the reaction time, k_r is the reaction rate constant, K is the adsorption coefficient of the reactant, K_s is the adsorption coefficient of the solvent, and C_s is the concentration of the solvent. When the reactant is more strongly adsorbed than solvent, Eq. 1 can be simplified to Eq. 2

$$r = -\frac{dC}{dt} = \frac{k_r KC}{1+KC} \tag{2}$$

When the initial concentration of reactant is very low ($KC << 1$), Eq. 2 can be further simplified to Eq. 3

$$r = -\frac{dC}{dt} = k_r KC = k_{app} C \tag{3}$$

where k_{app} represents the apparent reaction rate constant. According to Eq. 3, if the photocatalytic reaction can be described by the simplified L-H model, the reaction rate should be proportional to the concentration of RhB. To identify whether the photodegradation of RhB can be fitted by the L-H model or not, a set of experiments with different initial RhB concentrations have been conducted. The corresponding results are presented in Figure 7. As observed in Figure 7a, the RhB concentration decreased with the increase of the irradiation time. After 180 min, RhB solutions with initial concentrations varying from 2 to 8 mg/L were degraded almost completely. The relationship between the concentration of RhB and the irradiation time has been fitted by an exponential function. Equations of the fitting plots and their values of the coefficient of determination have been listed in Supporting Information, Table S1. As clearly shown, all values of the coefficient of determination are close to 1, which indicates a very good fitting.

To obtain the reaction rates, the derived functions of the RhB concentration with respect to UV light irradiation time have been deduced. Based on the results, the relationship between the

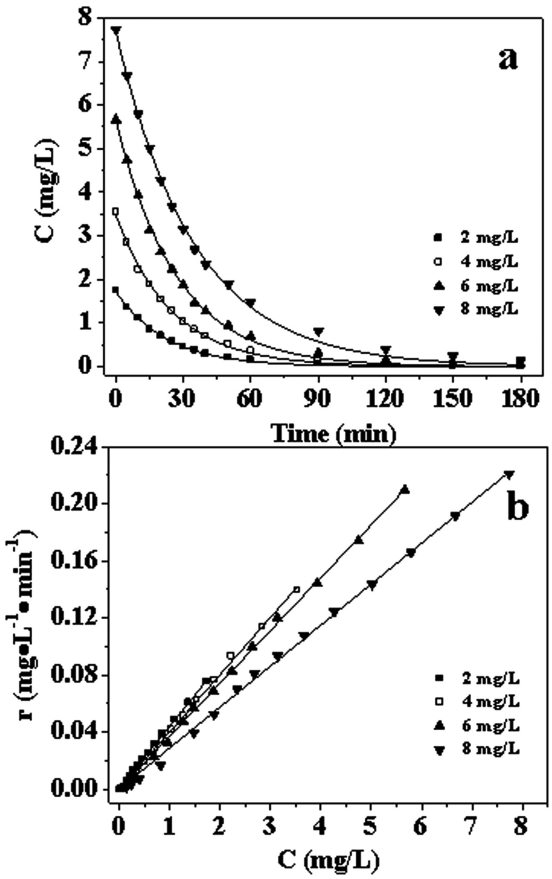

Figure 7. (a) The concentration of RhB as a function of UV light irradiation time and the corresponding fitting plots, and (b) the reaction rate of RhB as a function of the concentration of RhB and the corresponding fitting plots in the presence of the anatase TiO_2 nanotube arrays (The systems with different initial concentrations were placed in the dark for 30 min beforehand).

reaction rate of RhB and its concentration has been established, which is presented in Figure 7b. The values of the coefficient of determination are very close to 0.999, which indicates very good linear characteristics. On the basis of what has been discussed above, it is reasonable to consider that the photocatalytic reaction of RhB solution in the presence of the anatase TiO_2 nanotube arrays can be described by the simplified L-H model. That is, the reaction can be ascribed to pseudo-first-order kinetic model at these initial RhB concentrations.

According to Eq. 3, the slope of the fitting line represents the apparent reaction rate constant k_{app}. As observed from Figure 7b, k_{app} decreased with the increase of initial RhB concentration, which is consistent with the previous study.[32,33] One reason for this observation is that with the increase of initial RhB concentration, a larger percent of the light might be adsorbed by the RhB molecules rather than by the TiO_2 nanotube arrays. Another possible reason is that the photocatalytic reaction possesses the photonic nature. High concentration of RhB solution might saturate the TiO_2 surface and reduce the photonic efficiency.

Photocatalytic activity of different TiO_2 samples

Figure 8 presents the photocatalytic performance of the three different TiO_2 samples: anatase TiO_2 nanotube arrays, commercial anatase TiO_2 nanoparticle film, and TiO_2 nanotube arrays without post heating. For comparison, two blank tests (experiments of photolysis and adsorption under dark conditions) also have been conducted. As shown in Figure 8a, the degradation ratio of RhB in the presence of the anatase TiO_2 nanotube arrays, commercial anatase TiO_2 nanoparticle film, and the TiO_2 nanotube arrays without post heating is 99.3, 89.3, and 44.1%, respectively, whereas the RhB degradation ratio is only 18.8% in the absence of any photocatalyst. Curve S5 of Figure 8a shows the result of the adsorption experiment. As shown, the relative concentration of RhB decreased in the first 30 min, and then leveled off. The final adsorption ratio of RhB on the TiO_2 nanotube arrays was 7.9%. For TiO_2 nanotube arrays without post heating and commercial anatase TiO_2 nanoparticle film, their adsorption ratios were 22.7 and 7.8%, respectively.

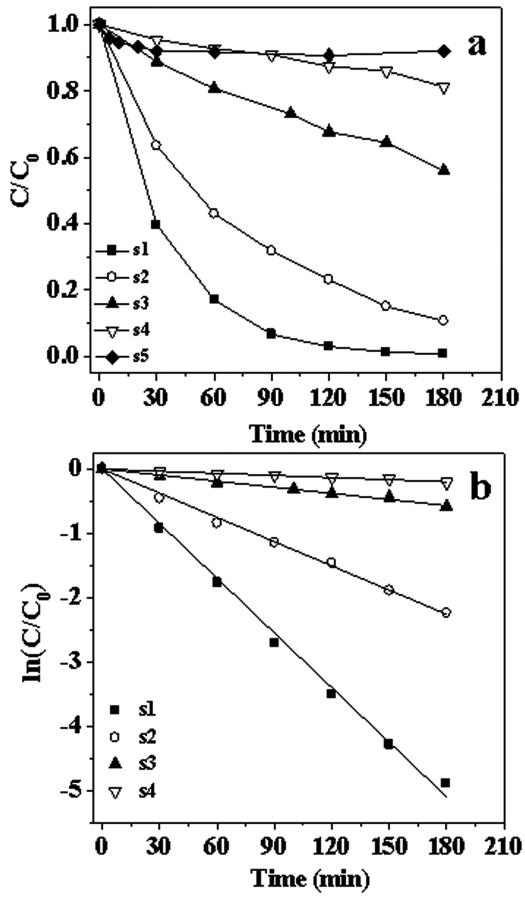

Figure 8. Photocatalytic degradation of RhB solution in the presence of (s1) the anatase TiO_2 nanotube arrays, (s2) commercial anatase TiO_2 nanoparticle film, (s3) TiO_2 nanotube arrays without post heating, and (s4) in the absence of any photocatalyst under UV light irradiation, and (s5) in the presence of the anatase TiO_2 nanotube arrays under dark conditions (C_0 and C are the concentrations of RhB solution at time $t = 0$ and $t = t$.

For s1-s4, the systems were placed in the dark for 30 min beforehand). (a) The variation of the relative concentration of RhB as a function of time and (b) the dependences of $\ln(C/C_0)$ on UV light irradiation time t and their fitting plots.

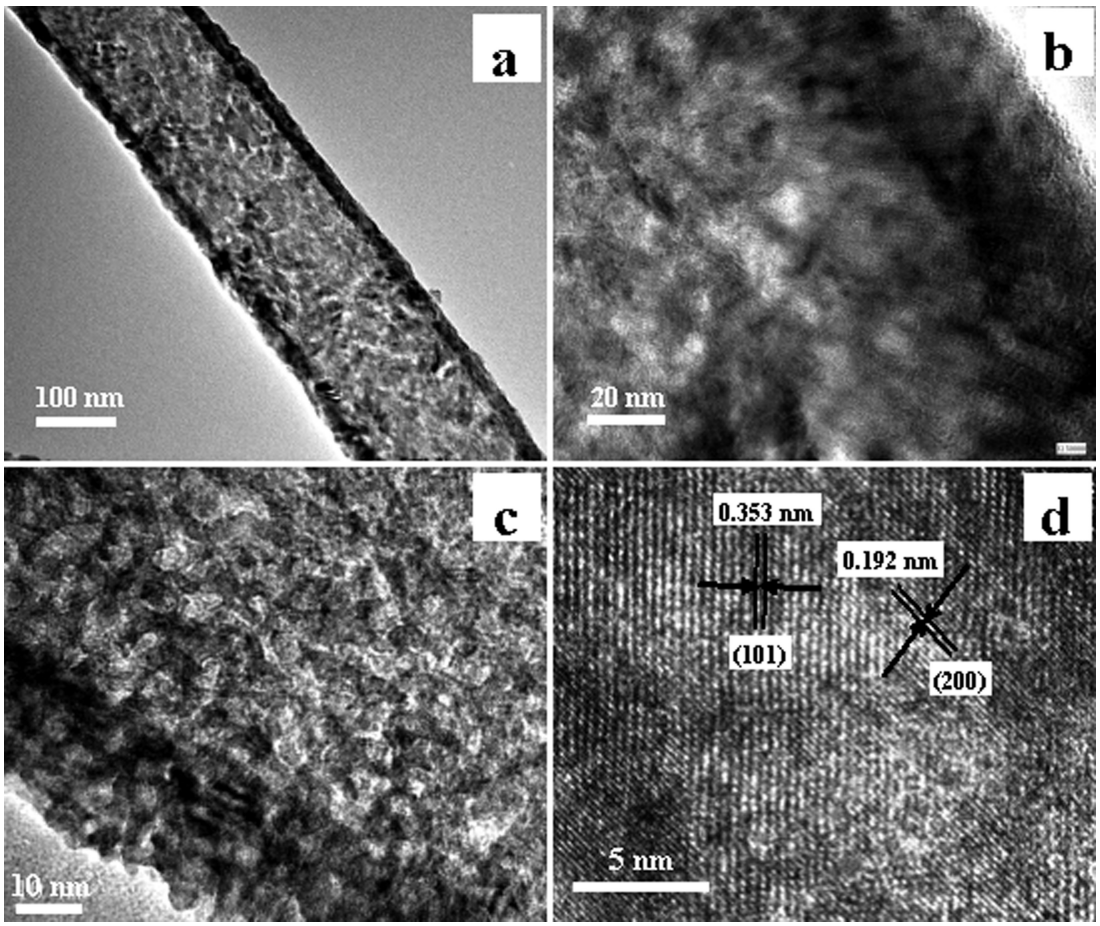

Figure 9. The TEM images (a–c) and HRTEM image (d) of the anatase TiO_2 nanotube.

As mentioned in the experimental section, before irradiation, the photocatalytic system was placed in the dark for 30 min. Therefore, the adsorption effect on the photocatalytic system can be eliminated. After removing the effect of direct photolysis, the contribution of the anatase TiO_2 nanotube arrays to the degradation ratio of RhB is 80.5%, indicating its predominant effect for decomposition of RhB.

According to the results in Figure 8b, it is also plausible to suggest that the reactions follow the simplified L-H model, which can also be written as $\ln(C_0/C) = k_{app}t$, where C_0 and C are the concentration of RhB solution at the moment $t = 0$ and $t = t$, respectively. The values of the apparent reaction rate constants for the three samples can be obtained. However, it is unreasonable to directly compare the values of the absolute apparent reaction rate constant without considering the film thickness and area, and the mass of active material. In our experiment, the film thicknesses of the TiO_2 nanotube arrays was about 15 μm, which is bigger than that of the commercial TiO_2 nanoparticle film (10 μm), and their film areas were all 1 cm^2. The active material mass of commercial TiO_2 nanoparticle film (1.68 mg) was much greater than that of the TiO_2 nanotube arrays (0.14 mg). Taking these factors into consideration, the values of the apparent rate constant were 12.16, 0.45, and 1.36 h^{-1} mg^{-1} cm^{-2} for the anatase TiO_2 nanotube arrays, commercial anatase TiO_2 nanoparticle film, and TiO_2 nanotube arrays without post heating, respectively. Apparently, the anatase TiO_2 nanotube arrays had the highest rate constant, indicating their highest photocatalytic activity in comparison with the other two samples.

To estimate the experimental error, the TiO_2 nanotube arrays annealed at 500°C for 2 h was selected as the photocatalyst for photodegradation of RhB because of their highest efficiency. A set of parallel experiments have been done to determine the error range. As shown in Supporting Information, Figure S7, the concentration of RhB decreased rapidly with the irradiation time. After 180 min, almost all the RhB was degraded. The experimental error is represented by the vertical line, which is approximately 8.1% at 30 min and decreases with the increased illumination time.

Characterization of microstructure

To understand the reasons for the enhanced photocatalytic performance of the anatase TiO_2 nanotube arrays, their microstructure was investigated by high-magnification TEM and HRTEM measurements. Figure 9a shows a nanotubular structure with a uniform wall thickness. Figures 9b, c exhibit higher magnification results, from which some irregular mesopores can be observed on the wall of the nanotube through the contrast between brightness and darkness. The pore size is about 10 nm. The HRTEM image of Figure 9d was recorded by focusing on one single crystal. Two types of lattice fringes can be clearly seen, indicating a good crystallinity. The lattice spacings are 0.353 and 0.192 nm, which correspond to the (101) and (200) planes of anatase TiO_2, respectively.

Table 1. Summary of the Specific Surface Area and Average Pore Size of TiO_2 Nanotubes without Post -Heating, Anatase TiO_2 Nanotubes, and Commercial Anatase TiO_2 Nanoparticles.

Sample	Specific Surface Area (m^2/g)	Average Pore Size (nm)
TiO_2 nanotubes without post heating	135.5	26.6
Anatase TiO_2 nanotubes	18.1	9.3
Commercial anatase TiO_2 naonoparticles	8.9	4.8

More detailed information on the structure of the three photocatalysts has been investigated by the nitrogen adsorption-desorption experiments, for which the TiO_2 nanotube samples were scrapped from the Cu substrates.

The N_2 adsorption-desorption results presented in, Supporting Information, Figure S8 display a type-IV isotherm with a hysteresis loop, indicating a mesoporous structure[34] of the TiO_2 nanotubes after and before post heating. Supporting Information, Figure S9 shows the N_2 absorption-desorption isothermal curves of commercial anatase TiO_2 nanoparticles. The value of specific surface area and average pore size of TiO_2 nanotubes without post heating, anatase TiO_2 nanotubes, and commercial anatase TiO_2 nanoparticles are listed in Table 1. As shown, their specific surface areas are 135.5, 18.1, and 8.9 m^2/g, respectively.

Without post heating, the TiO_2 nanotube was composed of large amounts of amorphous tiny grains, which led to a large specific surface area. Post heating at 500°C for 2 h resulted in the sintering of these tiny grains and turned them into larger crystals. Correspondingly, the specific surface area of the TiO_2 nanotubes had a sharp decrease. Commercial anatase TiO_2 nanoparticles showed the lowest specific surface area. Thermal treatment also led to the decrease of pore sizes of the TiO_2 nanotubes. The average pore size of the anatase TiO_2 nanotubes was 9.3 nm, which is consistent with the TEM observation in Figure 9b. For commercial anatase TiO_2 nanoparticles, they showed a small average pore size of 4.8 nm.

Recombination of electron-hole pairs

For semiconductor nanomaterials, the PL spectrum reflects the separation and recombination of photoinduced charge carriers. The lower the PL intensity, the lower the recombination rate of photogenerated electron-hole pairs, and the higher the photocatalytic activity of semiconductor photocatalysts.[35]

Figure 10 shows the PL spectra of the three samples (excitation wavelength: 300 nm. All samples for PL experiments had the same film area of 1 cm^2), all of which present an obvious emission at about 473 nm. It is clear that the anatase TiO_2 nanotube arrays showed the lowest PL intensity, whereas commercial anatase TiO_2 nanoparticle film showed the highest one. The TiO_2 nanotube arrays without post heating showed slightly higher PL intensity than the anatase TiO_2 nanotube arrays.

Taking the microstructure and PL properties of the samples into consideration, the possible reasons for the enhanced photocatalytic performance of the anatase TiO_2 nanotube arrays are listed as follows. First, one-dimensional TiO_2 nanotubular structure could provide a transport channel for charges along the longitudinal direction and make it possible to shorten the diffusion path for carriers and facilitate the charge separation.[19] On the other hand, the commercial anatase TiO_2 nanoparticle film was made up of randomly packed and interconnected anatase TiO_2 particles, and their disordered structure increased the opportunity for the charge recombination. In addition, the anatase TiO_2 nanotubes possessed a larger BET surface area than the commercial TiO_2 nanoparticles. Not only the outer surface but also the inner surface of the TiO_2 nanotubes could be used due to the mesoporous structure on the wall. These two factors might contribute to the better photocatalytic activity of the former. Although the TiO_2 nanotubes without post heating had a much larger BET surface than the anatase TiO_2 nanotubes, large amounts of structural defects on the nanotube walls due to low crystallization led to a higher recombination rate of electron-hole pairs. Consequently, the TiO_2 nanotube arrays without post heating showed a relatively poor photocatalytic performance in comparison with the anatase TiO_2 nanotube arrays.

Life cycle assessment of the anatase TiO_2 nanotube arrays

To examine the durability of the anatase TiO_2 nanotube arrays for water treatment, their life cycle assessment was performed. The corresponding results are presented in Figure 11. All the experiments were conducted under the same conditions (initial RhB concentration: 4 mg/L; UV light irradiation time: 3 h). After each run, the anatase TiO_2 nanotube arrays were cleaned with absolute ethanol and deionized water, respectively, and then dried in air. As observed, the RhB degradation ratio varied from 99.3% of the first run to 84.9% of the sixth run.

As expected, with the increased run cycles, some active sites on the surface of the nanotubes might have been occupied by the formed intermediates, which is unfavorable for the adsorption of RhB. Therefore, RhB could not adsorb on the surface of the nanotubes to participate in the photocatalytic reaction as effectively as at the beginning. This may explain why the degradation ratio of RhB decreased gradually with the increased run cycles. Nevertheless, the decrease of the RhB degradation ratio over the first six runs is small, and it can be considered that the anatase TiO_2 nanotube arrays possessed a good stability as a photocatalyst.

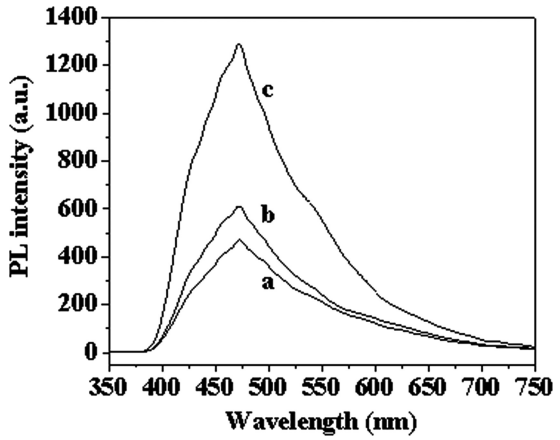

Figure 10. Photoluminescence spectra of the TiO_2 samples (excitation wavelength: 300 nm).

(a) Anatase TiO_2 nanotube arrays, (b) TiO_2 nanotube arrays without post heating, and (c) commercial anatase TiO_2 nanoparticle film.

Scale-up performance of the anatase TiO_2 nanotube arrays

To consider the potential feasibility of the anatase TiO_2 nanotube arrays for photocatalytic water treatment at large scale, different film areas of the anatase TiO_2 nanotube arrays with similar quality were successfully prepared, including 1, 2, and 4 cm^2 (see Supporting Information, Figure S10). Figure 12 presents the photocatalytic performance of the anatase TiO_2 nanotube arrays in various scale-up systems. When the photocatalyst film area and the volume of the RhB solution were both scaled up eight times, the degradation ratio of RhB still reached up to 92.1%.

The performance of the anatase TiO_2 nanotube arrays at different scales demonstrates that the process may be operated at large scale for the potential engineering applications. With increase of the scale, the small drop in the photocatalytic efficiency might be ascribed to the more pronounced effect of the mass transfer on the overall reaction rate. Further study is required to understand the effect of the mass transfer at different scales, which remains to be future work.

It should also be noted that the copper substrate used is alkali sensitive. In practice, wastewater may have various pH values. Therefore, it is necessary to adjust the pH value of wastewater to neutral value before the TiO_2 nanotube array film can be used.

Conclusions

TiO_2 nanotube arrays with lengths of ~15 μm and diameters of 200–500 nm have been successfully prepared with $Cu(OH)_2$ nanorods grown on the copper substrate as sacrificial templates. This route involves outward coating of TiO_2 and inward etching of $Cu(OH)_2$ cores. The performance of the anatase TiO_2 nanotube arrays for photocatalytic degradation of RhB in aqueous solution has been proved to be superior to that of TiO_2 nanotube arrays without post heating and commercial anatase TiO_2 nanoparticle film. Furthermore, the anatase TiO_2 nanotube arrays had a good durability and a satisfactory photocatalytic performance in scale-up systems. It is believed that this study has opened a new avenue to fabricate free-standing TiO_2 nanotube arrays in large scale. In comparison with commonly used powder-form photocatalysts, the anatase TiO_2 nanotube arrays grown on substrates had the advantages of easy recovery and stable structure. They also effectively overcame the problem concerning the decreasing active surface areas caused by immobilization of powder-form photocatalysts. The scale-up experiments demonstrated the potential engineering application of using the anatase TiO_2 nanotube arrays for wastewater treatment.

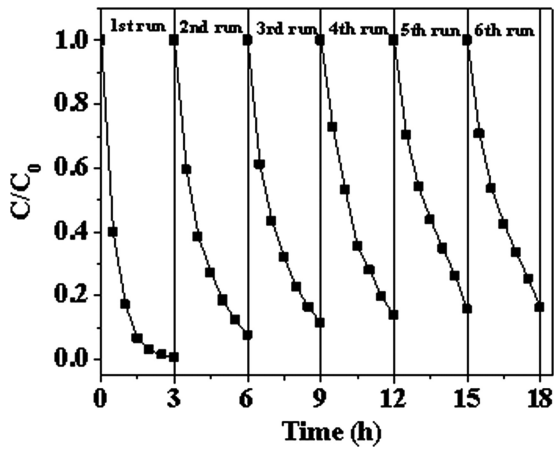

Figure 11. Life cycle performance of the anatase TiO_2 nanotube arrays in the photocatalytic degradation of RhB solution under UV light irradiation.

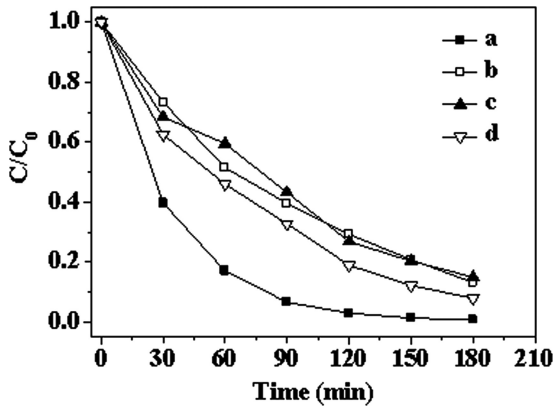

Figure 12. Comparison of photocatalytic performance of the anatase TiO_2 nanotube arrays in various scale-up systems.

The area of the TiO_2 nanotube arrays and the corresponding volume of RhB solution treated (a) 1 cm^2, 1 mL; (b) 2 cm^2, 2 mL; (c) 4 cm^2, 4 mL; (d) 2 × 4 cm^2, 8 mL (The systems were placed in the dark for 30 min beforehand).

Acknowledgments

This work is supported by the National Natural Science Foundation of China (NSFC Grants 20976033, 21176054, and 21271058), the Fundamental Research Funds for the Central Universities (2010HGZY0012), and the Education Department of Anhui Provincial Government (TD200702). The authors are grateful to Prof. Zhibing Zhang of the University of Birmingham in UK for his advice and assistance.

Literature Cited

1. Albu SP, Ghicov A, Macak JM, Hahn R, Schmuki P. Self-organized, free-standing TiO_2 nanotube membrane for flow-through photocatalytic applications. *Nano Lett*. 2007;7:1286–1289.
2. Chen SL, Wang AJ, Hu CT, Dai C, Benziger JB. Enhanced photocatalytic performance of nanocrystalline TiO_2 membrane by both slow photons and stop-band reflection of photonic crystals. *AlChE J*. 2012;58:568–572.
3. Prasad GK, Mahato TH, Singh B, Ganesan K, Srivastava AR, Kaushik MP, Vijayraghavan R. Decontamination of sulfur mustard and sarin on titania nanotubes. *AlChE J*. 2011;54:2957–2963.
4. Lin SW, Li DG, Wu J, Akbar SA, Li XG. A selective room temperature formaldehyde gas sensor using TiO_2 nanotube arrays. *Sens Actuators B*. 2011;156:505–509.
5. Varghese OK, Gong DW, Paulose M, Ong KG, Grimes CA. Hydrogen sensing using titania nanotubes. *Sens Actuators B*. 2003;93:338–344.
6. Mor GK, Shankar K, Paulose M, Varghese OK, Grimes CA. Use of highly-ordered TiO_2 nanotube arrays in dye-sensitized solar cells. *Nano Lett*. 2006;6:215–218.
7. Xu JW, Jia CH, Cao B, Zhang WF. Electrochemical properties of anatase TiO_2 nanotubes as an anode material for lithium-ion batteries. *Electrochim Acta*. 2007;52:8044–8047.
8. Wang DW, Fang HT, Li F, Chen ZG, Zhong QS, Lu GQ, Cheng HM. Aligned titania nanotubes as an intercalation anode material for hybrid electrochemical energy storage. *Adv Funct Mater*. 2008;18:3787–3793.

9. Chen JS, Lou XW. Anatase TiO_2 nanosheet: an ideal host structure for fast and efficient lithium insertion/extraction. *Electrochem Commun*. 2009;11:2332–2335.
10. Jiu JT, Isoda SJ, Wang F, Adach M. Dye-sensitized solar cells based on a single-crystalline TiO_2 nanorod film. *J Phys Chem B*. 2006;110:2087–2092.
11. Shin Y, Lee S. Self-organized regular arrays of anodic TiO_2 nanotubes. *Nano Lett*. 2008;8:3171–3173.
12. Wang J, Lin ZQ. Freestanding TiO_2 nanotube arrays with ultrahigh aspect ratio via electrochemical anodization. *Chem Mater*. 2008;20:1257–1261.
13. Ding SJ, Chen JS, Wang ZY, Cheah YL, Madhavi S, Hub X, Lou XW. TiO_2 hollow spheres with large amount of exposed (001) facets for fast reversible lithium storage. *J Mater Chem*. 2011;21:1677–1680.
14. Zhang WX, Yang SH. In situ fabrication of inorganic nanowire arrays grown from and aligned on metal substrates. *Acc Chem Res*. 2009;42:1617–1627.
15. Rani S, Roy SC, Paulose M, Varghese OK, Mor GK, Kim S, Yoriya S, LaTempa TJ, Grimes CA. Synthesis and applications of electrochemically self-assembled titania nanotube arrays. *Phys Chem Chem Phys*. 2010;12:2780–2800.
16. Rachel A, Subrahmanyamb M, Boule P. Comparison of photocatalytic efficiencies of TiO_2 in suspended and immobilised form for the photocatalytic degradation of nitrobenzenesulfonic acids. *Appl Catal B*. 2002;37:301–308.
17. He C, Li XZ, Grahama N, Wang Y. Preparation of TiO_2/ITO and TiO_2/Ti photoelectrodes by magnetron sputtering for photocatalytic application. *Appl Catal A: Gen*. 2006;305:54–63.
18. Bessergenev VG, Pereira RJF, Mateus MC, Khmelinskii IV, Vasconcelos DA, Nicula R, Burkel E, Botelho do Rego AM, Saprykin AI. Study of physical and photocatalytic properties of titaniumdioxide thin films prepared from complex precursors by chemical vapour deposition. *Thin Solid Films*. 2006;503:29–39.
19. Macak JM, Zlamal M, Krysa J, Schmuki P. Self-organized TiO_2 nanotube layers as highly efficient photocatalysts. *Small*. 2007;3:300–304.
20. Zwilling V, Aucouturier M, Darque-Ceretti E. Anodic oxidation of titanium and TA6V alloy in chromic media. *An electrochemical approach. Electrochim Acta*. 1999;45:921–929.
21. Wang JS, Cui YT, Li HY, Wang ZZ, Huang KL, Sun GS. In situ synthesis and characterization of TiO_2 nanoarray films. *Res Chem Intermed*. 2010;36:17–26.
22. Zhang WX, Xu J, Yang ZH, Ding SX. Mesoscale organization of Cu_7S_4 nanowires: formation of novel sheath-like nanotube array. *Chem Phys Lett*. 2007;434:256–259.
23. Xu J, Zhang WX, Yang ZH, Yang SH. Lithography inside $Cu(OH)_2$ nanorods: a general route to controllable synthesis of the arrays of copper chalcogenide nanotubes with double walls. *Inorg Chem*. 2008;47:699–704.
24. Chen Z, Wang ZL, Zhan P, Zhang JH, Zhang WY, Wang HT, Ming NB. Preparation of metallodielectric composite particles with multishell structure. *Langmuir*. 2004;20:3042–3046.
25. Wang ZL, Mao LQ, Lin J. Preparation of TiO_2 nanocrystallites by hydrolyzing with gaseous water and their photocatalytic activity. *J Photochem Photobiol A*. 2006;177:261–268.
26. Zhang ZH, Yuan Y, Shi GY, Fang YJ, Liang LH, Ding HC, Jin LT. Photoelectrocatalytic activity of highly ordered TiO_2 nanotube arrays electrode for azo dye degradation. *Environ Sci Technol*. 2007;41:6259–6263.
27. Sun Q, Xu YM. Evaluating intrinsic photocatalytic activities of anatase and rutile TiO_2 for organic degradation in water. *J Phys Chem C*. 2010;114:18911–18918.
28. Zhou SH, Ray AK. Kinetic studies for photocatalytic degradation of eosin B on a thin film of titanium dioxide. *Ind Eng Chem Res*. 2003;42:6020–6033.
29. Chen DW, Li FM, Ray AK. Effect of mass transfer and catalyst layer thickness on photocatalytic Reaction. *AIChE J*. 2000;5:1034–1045.
30. Wang XH, Li JG, Kamiyama H, Moriyoshi Y, Ishigaki T. Wavelength-sensitive photocatalytic degradation of methyl orange in aqueous suspension over iron(III)-doped TiO_2 nanopowders under UV and visible light irradiation. *J Phys Chem B*. 2006;110:6804–6809.
31. Krysa J, Waldner G, Mnkova H, Jirkovsky J, Grabner G. Photocatalytic degradation of model organic pollutants on an immobilized particulate TiO_2 layer roles of adsorption processes and mechanistic complexity. *Appl Catal B*. 2006;64:290–301.
32. Wang PH, Zhou T, Wang R, Lim TT. Carbon-sensitized and nitrogen-doped TiO_2 for photocatalytic degradation of sulfanilamide under visible-light irradiation. *Water Res*. 2011;45:5015–5026.
33. Chong MN, Jin B, Chow CWK, Saint C. Recent developments in photocatalytic water treatment technology: a review. *Water Res*. 2010;44:2997–3027.
34. Sing KSW, Everett DH, Haul RAW, Moscou L, Pierotti RA, Rouquerol J, Siemieniewska T. Reporting physisorption data for gas solid systems with special reference to the determination of surface-area and porosity. *Pure Appl Chem*. 1985;57:603–619.
35. Jing LQ, Fu HG, Wang BQ, Wang DJ, Xin BF, Li SD, Sun JZ. Effects of Sn dopant on the photoinduced charge property and photocatalytic activity of TiO_2 nanoparticles. *Appl Catal B*. 2006;62:282–291.

Manuscript received Apr. 10, 2012, and final revision received Nov. 26, 2012